Appendix A—NSHMP Block Model of Western United States Active Tectonics

By R. McCaffrey,[1] P. Bird,[2] J. Bormann,[3] K.M. Haller,[4] W.C. Hammond,[3] W. Thatcher,[5] R.E. Wells,[5] Y. Zeng[4]

[1]Dept. of Geology, Portland State University, Portland, Oreg.
[2]Dept. of Earth and Space Sciences, University of California, Los Angeles, Calif.
[3]Nevada Geodetic Laboratory, University of Nevada Reno, Nev.
[4]USGS Golden, Colo.
[5]USGS Menlo Park, Calif.

Abstract

We developed a block model of active faults in the Western United States (WUS) in support of the 2014 National Seismic Hazards Mapping Project (NSHMP14). The block model used a modified 2008 fault-source model as block boundaries as much as reasonably possible with the aim of estimating slip rates on those faults. Global positioning system (GPS)-derived horizontal velocity data were compiled from seven regional solutions and rotated into a common North American reference frame. The GPS velocities were edited to remove outliers, and a correction was made to account for elastic strain rates caused by locking on the Cascadia subduction zone. The GPS velocity field was used by researchers to assess, and if necessary, modify fault slip rates in the modified 2008 fault-source model. Block models resulted in generally faster fault slip rates than assigned in the modified 2008 fault-source model.

Introduction

Block models of crustal deformation allow analysis and simultaneous interpretation of multiple types of data that relate to motions of the crust and slip rates on faults. The models are based on plate tectonic formulations; that is, crustal blocks, like tectonic plates, rotate about Euler poles. In addition, the block models can account for elastic strain rates that occur near faults due to friction on them and distributed strain rates that result from slip on multiple, closely spaced faults. Elastic-strain-rate corrections are needed to interpret decade-scale global positioning system (GPS) velocity data in terms of longer term fault motions. This appendix reports on the development of the Western United States (WUS) block model WUS5 used to interpret GPS velocity data in the context of fault slip rates assigned in the modified 2008 NSHMP source model.

Block Model WUS5

We developed a block model, called WUS5 that includes 70 blocks in the WUS (fig. A-1). To maintain continuity with UCERF3 (Uniform California Earthquake Rupture Forecast, version 3), this model also includes the blocks in California used in the UCERF3 average block model (ABM), but the number of fault segments was decreased for simplicity. In WUS5, the block boundaries outside California were greatly modified from those used in UCERF3.

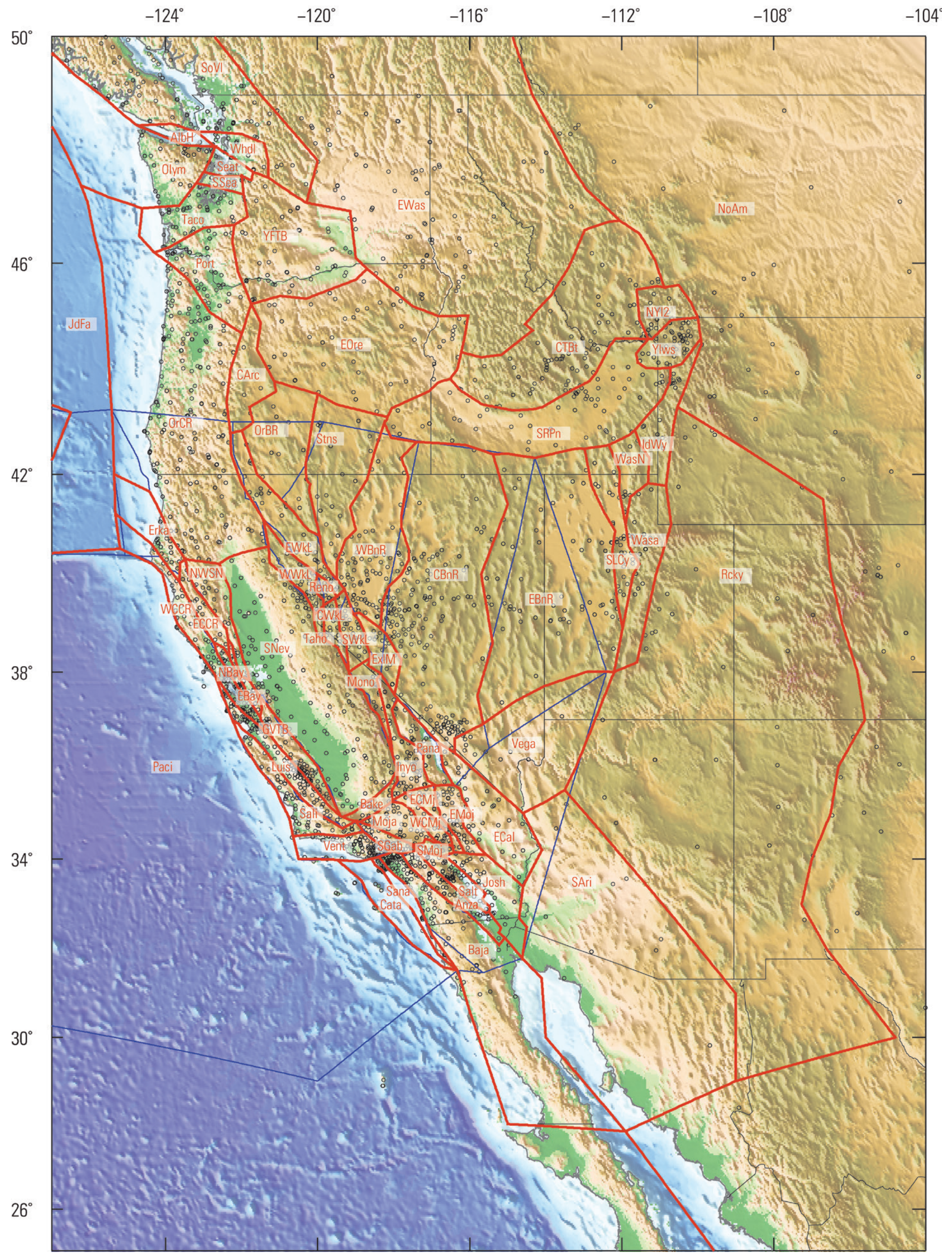

Figure A-1. Map of Western United States (WUS) showing block boundaries for WUS5 (red) and California's UCERF3 ABM (Uniform California Earthquake Rupture Forecast, version 3, average block model) (blue). Black dots show locations of global positioning system velocities used. Four-letter codes are block names.

The initial block model was adapted from those of McCaffrey (2005) and Meade and Hager (2005) for California, McCaffrey and others (2007) for the Pacific Northwest, Payne and others (2008, 2012) for the Wasatch and Snake River Plain region, Hammond and others (2011) for the Walker Lane area, and Kreemer and others (2010) for the southern Great Basin. The initial model was modified to connect the separate regions and to follow more closely the set of NSHMP14 target faults (fig. A-2). The block boundaries include most NSHMP14 faults with slip rates of greater than 1 mm/yr. Other modifications were to break up the original long, thin blocks, within which motions are difficult to resolve, into smaller entities. Block boundaries were used to separate regions of differing strain rates even though we did not always believe the boundaries themselves are areas of significant slip; in these cases some models included estimates of the off-fault strain rates, which are not included in the modified 2008 NSHMP source model.

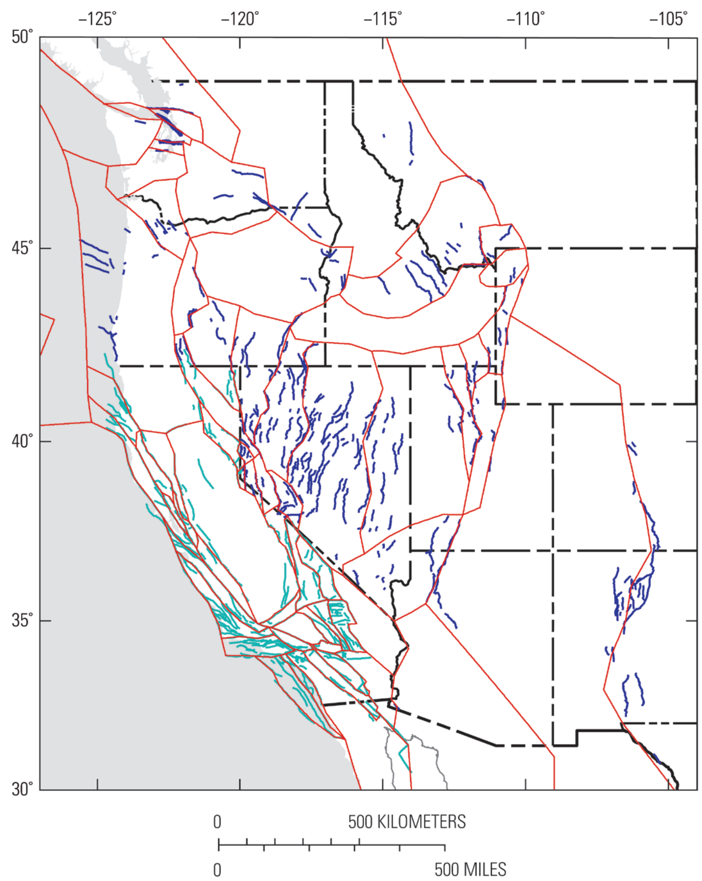

Figure A-2. Block-model boundaries (red lines) and National Seismic Hazards Mapping Project fault sources. Turquoise lines represent UCERF3 (Uniform California Earthquake Rupture Forecast, version 3) faults; blue lines represent faults in study area.

In many regions, GPS data cannot distinguish between slip on multiple, closely spaced individual faults and more uniformly distributed strain rates. For example, as Payne and others (2012) show, the CTBt block (fig. A-2), north of the Snake River Plain, could be subdivided along known faults (Lemhi, Beaverhead, Lost River, and so forth), but in doing so, the fit to the GPS data does not change. Hence the GPS velocities do not provide additional information on the slip rates of these faults. There are many similar examples throughout the WUS, most notably the Basin and Range of Nevada where we assigned block boundaries based on perceived spatial changes in strain rates but without expectation to constrain slip rates on them.

GPS Data

GPS velocities were compiled from seven velocity fields, listed in table A-1 and shown in figure A-3A. Some of the velocity fields encompassed the entire boundary, whereas others were more regional in scale.

Table A-1. Velocity fields used and rotation into North American reference frame.

[GPS (global positioning system) is the number of velocities in the solution. Longitude, latitude, and omega give the Euler pole used to rotate the velocity field into the North American reference frame. PBO (Plate Boundary Observatory), PANGA (Pacific Northwest Geodetic Array), and SOPAC (Scripts Orbit and Permanent Array Center) access date in Reference column]

Field	GPS	Longitude	Latitude	Omega	Reference
PNW	696	282.1	24.9	0.022	McCaffrey and others (2013)
CMM4	551	285.3	35.3	0.020	Shen and others (2011)
PBO	942	331.0	–40.0	0.014	PBO 2011.08.01
UNR	219	273.9	–2.9	0.184	Hammond and others (2011)
PANGA	308	299.6	43.0	0.023	PANGA 2012.03.05
SOPAC	1252	273.5	–4.9	0.185	SOPAC 2012.07.06
SHEN	1997	69.1	–18.4	0.011	Z-K Shen, unpublished

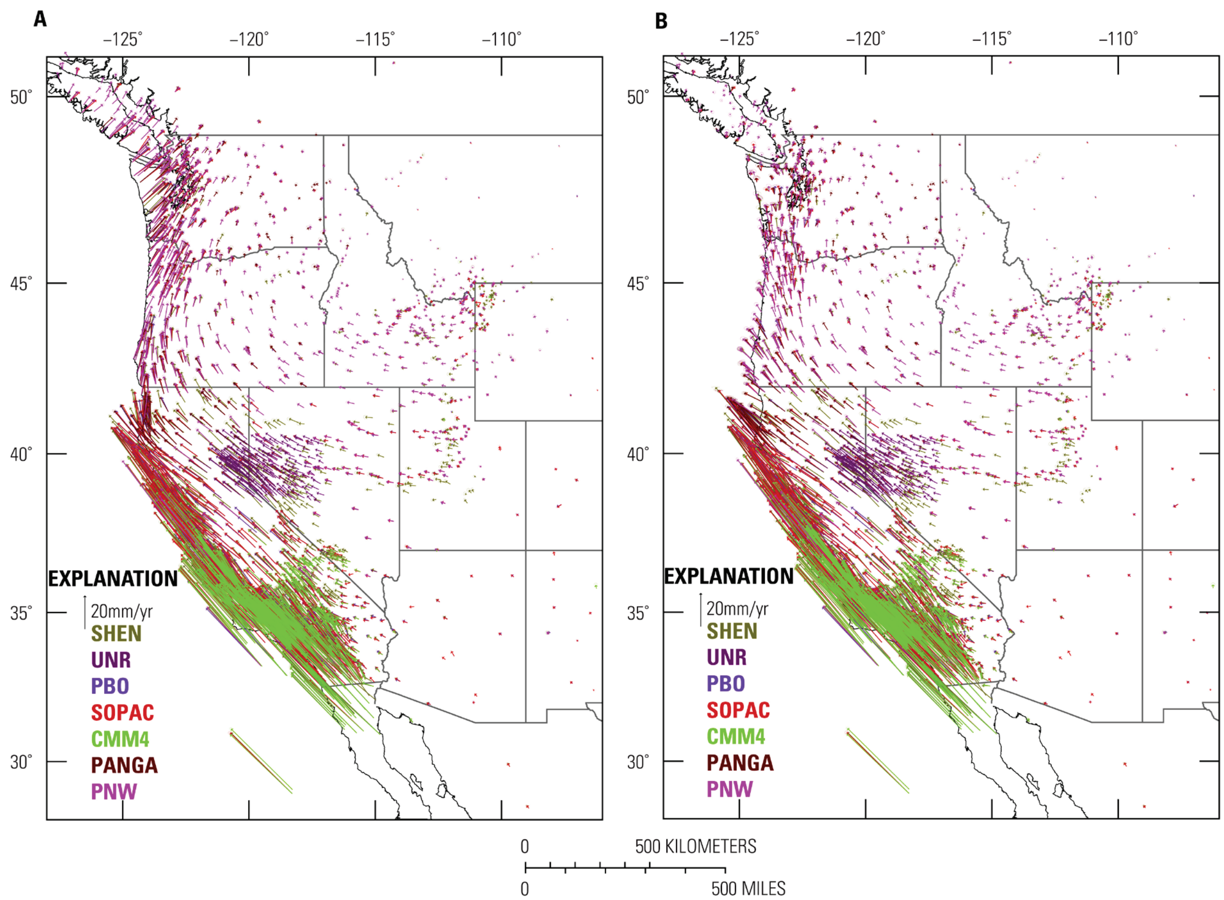

Figure A-3. Maps of global positioning system (GPS) velocity field data for the Western United States. *A*, Original velocity fields rotated into North American reference frame. *B*, Corrected velocity fields with effects of Cascadia subduction-zone locking removed. Vector colors correspond to source in table A-1.

In addition to the GPS velocities, for which we used only the horizontal components in the block modeling, vertical velocities derived from leveling surveys (Burgette and others, 2009) were used to help constrain the locking on the Cascadia subduction fault (see McCaffrey and others, 2013, for details). The vertical rates were not distributed with the corrected horizontal velocities or used in subsequent modeling.

Reference Frame

Using the block model WUS5 and the inversion program *tdefnode* (McCaffrey, 2002, 2009), the velocity fields were rotated into a common reference frame defined by the North American (NoAm) block. This is accomplished by rotating each velocity field to minimize the velocities of the GPS sites on the reference (NoAm) block. For velocity fields that have no or few sites on NoAm, the reference frame rotations result from aligning it with the other velocity fields. To get the rotation of a velocity field (V) relative to NoAm (N), we solve:

$$_{V}\Omega_{N} = {}_{V}\Omega_{B} + {}_{B}\Omega_{N} \qquad (1)$$

where B represents a block. Because $_{B}\Omega_{N}$ is the same for all velocity fields, $_{V}\Omega_{B}$ is estimated by minimizing the velocity residuals for velocity field V in the block B. And because $_{V}\Omega_{N}$ is the same for all blocks, it is estimated by minimizing velocity residuals in all the blocks. In the inversion, only $_{V}\Omega_{N}$ and $_{B}\Omega_{N}$ are estimated. Using this approach, the velocity fields do not require common sites, and not all need sites on the reference block. Each velocity field, however, must cover multiple blocks.

Most of the velocity fields used were already close to being in the North American reference frame and needed only small adjustments, on the order of 1 mm/yr or less, to align with the average field. Two fields (University of Nevada, Reno, UNR and Scripts Orbit and Permanent Array Center, SOPAC; table A-1 and fig. A-3) were initially in a global International Terrestrial Reference Frame (ITRF) and required adjustments of closer to 15 mm/yr (the adjustments are by rotations so will vary across the network).

Data Editing

After initial runs of the block model, during which the velocity fields were rotated into a common reference frame, the velocities were edited by visual inspection and by examining the statistics and misfits. For mature velocity fields, in the absence of co-seismic signals, the velocities vary spatially in a very smooth manner. Hence, if a single velocity was very different from nearby velocities in either azimuth or magnitude or both, we removed it from the dataset. In other cases, the deviation of a velocity was not visually obvious but was statistically different from nearby velocities, and it was removed.

We also excluded velocities with high uncertainties because they add little information in a least-squares inversion. The uncertainty cutoffs applied were 0.8 mm/yr for PNW and UNR fields (table A-1) and 1.0 mm/yr for the others. In addition we applied a “floor” to the uncertainties in the sense that any formal uncertainty of less than 0.3 mm/yr was set to 0.3 mm/yr. This limitation was aimed to avoid sites with very low uncertainties, some less than 0.1 mm/yr, from dominating the least-squares solution. It also represents some expected level of uncertainty among the reference frames. We removed “equated” sites from some of the solutions; these are nearby sites where data were combined in the GAMIT/GLOBK velocity analysis (*http://www-gpsg.mit.edu/~simon/gtgk/*) to estimate a single velocity and uncertainty. Sites within about 30 km of five actively deforming volcanic regions were also removed (Mount Saint Helens, Mono Lake, Rainier, Shasta, and Sisters).

Cascadia Elastic Strain-Rate Correction

Locking on the Cascadia subduction zone was estimated by inverting the horizontal GPS and vertical leveling data (fig. A-4). The details of the procedure are outlined in McCaffrey and others (2013), but in this application we used all seven velocity fields. The geometry of the Cascadia plate interface was taken from McCrory and others (2003). The elastic velocities due to fault locking were calculated using dislocations in an elastic half-space following Okada (1985) and using the Savage (1983) backslip approach; the backslip component is $-\varphi\mathbf{V}$ where φ is a locking fraction and $\mathbf{V}$ is the relative motion vector across the fault. The vector $\mathbf{V}$ is derived from the blocks' Euler poles and φ is estimated in the inversion. For this calculation we parameterized the distribution of the locking fraction φ with a defined function describing the change in locking with depth along profiles down the dip of the slab interface. The parameterization follows Wang and others (2003); $\varphi = 1.0$ at depths shallower than the top, z_u, of what they call the effective transition zone (ETZ) and $\varphi = 0.0$ at depths below the bottom, z_l , of the ETZ. Within the ETZ

$$\varphi(z) = [\exp(-z'/\gamma) - \exp(-1/\gamma)]/[1 - \exp(-1/\gamma)] \qquad (2)$$

where $z' = (z - z_u) / (z_l - z_u)$ and γ is a shape factor. McCaffrey and others (2007) modified Wang's representation to allow for a more general case. Equation (2), in addition to constraining φ to decrease with depth, forces the slope $d\varphi/dz$ to increase or remain approximately constant with depth (fig. 8 in Wang and others, 2003). To allow the slope to decrease with depth, we use a new parameter, γ', and make the substitution in (2) of $\gamma = \gamma'$ when $\gamma' \leq 5$, and $\gamma = \gamma' - 10$ when $5 < \gamma' \leq 10$. For values of γ' between 0 and 5, $\varphi(z)$ is given by (2), and for γ' between 5 and 10, $\varphi(z)$ is (2) reflected about the φ and z axes (fig. 7a in McCaffrey and others, 2007).

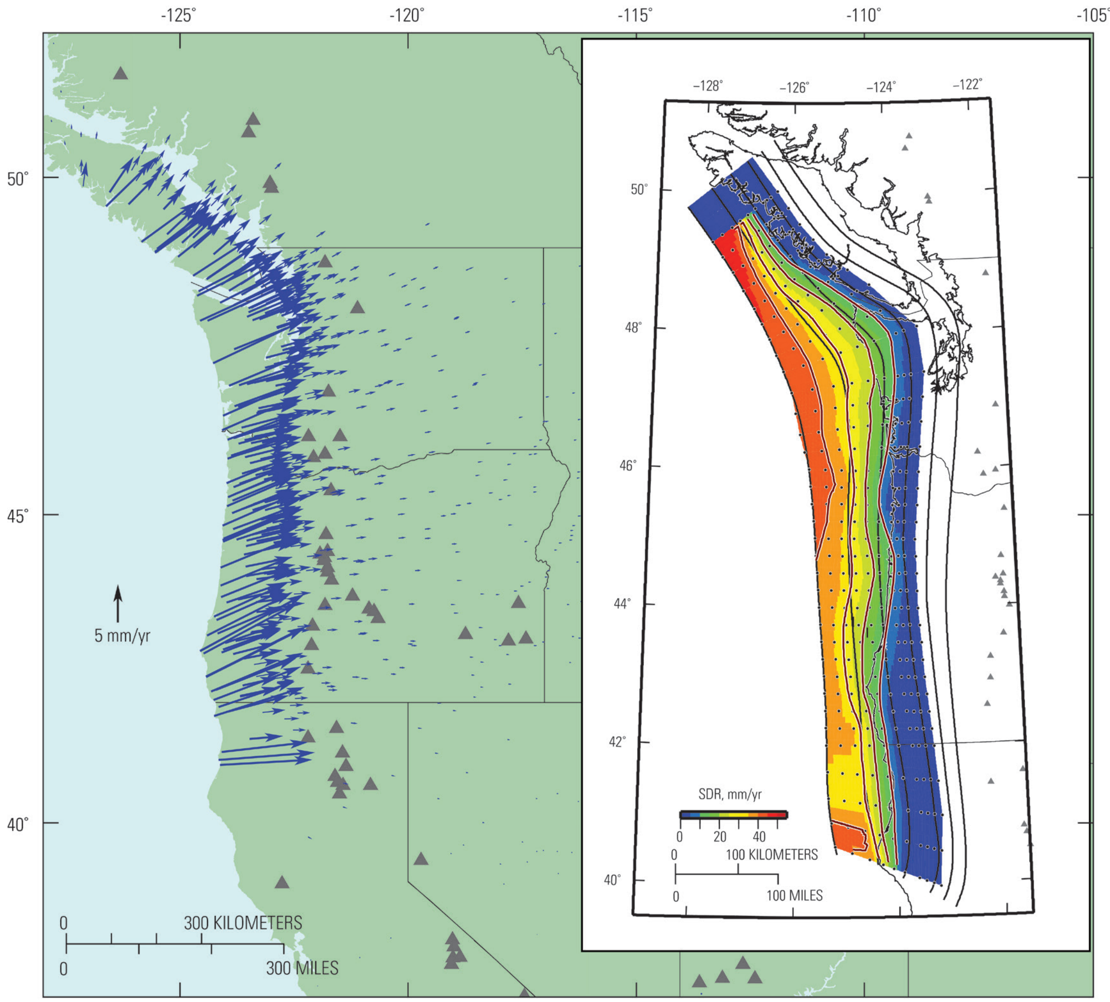

Figure A-4. Corrections to velocity field for locking at the Cascadia subduction zone. Insert shows locking model; SDR is the slip-deficit rate; dots are node positions; black lines are 10-kilometer slab contours and red lines are 10 millimeter per year (mm/yr) SDR contours. Triangles represent volcano locations.

The Cascadia slab interface was divided into 34 profiles starting at the deformation front, running perpendicular to it, and in the down-dip direction. The profiles were then discretized by node positions in longitude, latitude, and depth; the value of φ was estimated at each node (depth) following the function (2). In the inversion, the parameters γ', z_l, and z_u were estimated for each profile, subject to along-strike smoothing. Smoothing is applied by using a penalty function to damp the Laplacian of the φ distribution (McCaffrey and others, 2013). The "best-fit" set of parameters was found by minimizing the sum of the data misfit (reduced chi-square) plus the penalty function.

The model used to estimate Cascadia locking included all the blocks (fig. A-1) while solving for their angular velocities but not internal strain within them. The motion of the Juan de Fuca plate (JdFa) was estimated in the inversion using spreading rates at the Juan de Fuca Ridge (DeMets and others, 2010) and fixing the Pacific-North America pole. The motion of JdFa relative to the fore-arc blocks give the slip vector **V** used in the calculation of elastic strain at the Cascadia subduction zone. Once a best-fit set of parameters was determined, they were used to solve the forward problem to estimate a velocity at each GPS site arising from Cascadia locking (fig. A-4). These velocities were then subtracted from the observed site velocities and 10 percent of the locking velocities were added to the velocity uncertainties as follows:

$$\sigma_{new} = \sqrt{[\ \sigma^2_{old} + (0.10 * V_{lock})^2]} \quad (3)$$

The resulting corrected velocity field is shown in figure A-3*B*.

Geologic Slip Rates

In block models, geologic data, that is, estimated or observed slip rates on faults by geologic means, can be used to constrain the motions of blocks in a formal inversion because the fault slip rate is simply the relative motions of the blocks across the boundary. The WUS5 block model does not provide a one-to-one correspondence between the modified 2008 NSHMP source model based on expert analysis of geologic slip-rate data and block boundaries (fig. A-2), largely for the reason noted above. Block models cannot provide unique information on closely spaced faults, and therefore, not every fault is represented in a block model. Even using strain rates within the blocks does not permit a unique slip-rate estimate on the interior faults. Models that report slip rates on closely spaced faults are not strictly basing those rates on GPS data.

The source of geologic rates was the 2008 NSHMP source model with a few updates (Haller and Wheeler, 2008a,b; table 1 this volume). For the block models that include only horizontal long-term motions, the fault-parallel slip rates were converted to horizontal (heave) rates assuming the dip angles given in the modified 2008 NSHMP source model. For comparison with the other model results, the model predicted horizontal rates V_h were converted back to along-dip-slip rates V_{ds} using the same dip angles; $V_{ds} = V_h$/cosine (dip). Unfortunately, most of the fault slip rates were estimated from throw observations with little knowledge of dip angles; thus, the horizontal rates used in the block modeling are poorly constrained. Also available to the modeling were fault slip rates calculated by Bird (appendix C), using the technique described by Bird (2007), and rates taken from the literature and listed in McCaffrey and others (2007).

Block-Model Results with *tdefnode*

The WUS5 block model was run using the inversion program *tdefnode*, which is a modification of *defnode* (McCaffrey, 2002, 2009). Two runs were done, one of the entire WUS5 model and another that excluded California (WUS5-noCA; table A-2). As noted above, the representation of the UCERF-3 block model in California was coarsened, so the fit to the data was degraded. The reduced chi-square $\chi\eta^2$ misfit is large for these models compared with single-velocity field models of the U.S. Pacific Northwest, which typically have $\chi\eta^2$ less than ≈2 (McCaffrey and others, 2013). We attribute this to the use of multiple velocity fields that estimate velocities and uncertainties in different ways and to a heterogeneous set of observed fault slip rates.

Table A-2. Model run statistics.

[GPS (global positioning system) and SR (slip rate) give the number of GPS and slip-rate observations, respectively. Nrms is the normalized root mean square of the misfit to the data type. The reduced chi-square is $\chi\eta^2$]

Model	GPS/Nrms	SR/Nrms	#Parameters	$\chi\eta^2$
WUS5	12,385/3.1	1,028/4.2	564	10.4
WUS5-noCA	6,821/2.1	424/4.2	353	5.2

Slip Rates Derived from Block Model

The block model was used by two groups to estimate fault slip rates; McCaffrey (hereafter referred to as RM) used *tdefnode* (McCaffrey 2002, 2009) and Hammond and Bormann (appendix B; hereafter referred to as HB) used the method described in Hammond and others (2011). The block models made estimates for 114 of the 294 faults in the modified 2008 NSHMP source model, including most of those with published slip rates exceeding 1 mm/yr. The two inversions used the same block geometry and fault dips and generally the same formulation but differed in details of the implementation and the data (appendix B). A major difference was the level of off-fault strain rates allowed within the block. The RM model allowed more strain within blocks than did HB resulting in faster fault slip rates in the HB model (fig. A-5*A*). Both block inversions resulted in generally faster slip rates than in the modified 2008 NSHMP source model (figs. A-5*B* and A-5*C*). This latter result suggests that the GPS velocity fields may be indicating more total moment on faults than is implied by the modified 2008 NSHMP source model. This result is consistent with the Zeng and Shen fault-based inversion (appendix D) that forces a fit to the source model slip rates and estimated much higher off-fault moment rates than models that did not (appendix E)—a full 10 times more than the HB model. Hence, there is information in the geodetic data that is not incorporated into NSHMP14, which should be among the targets of research prior to the next NSHMP.

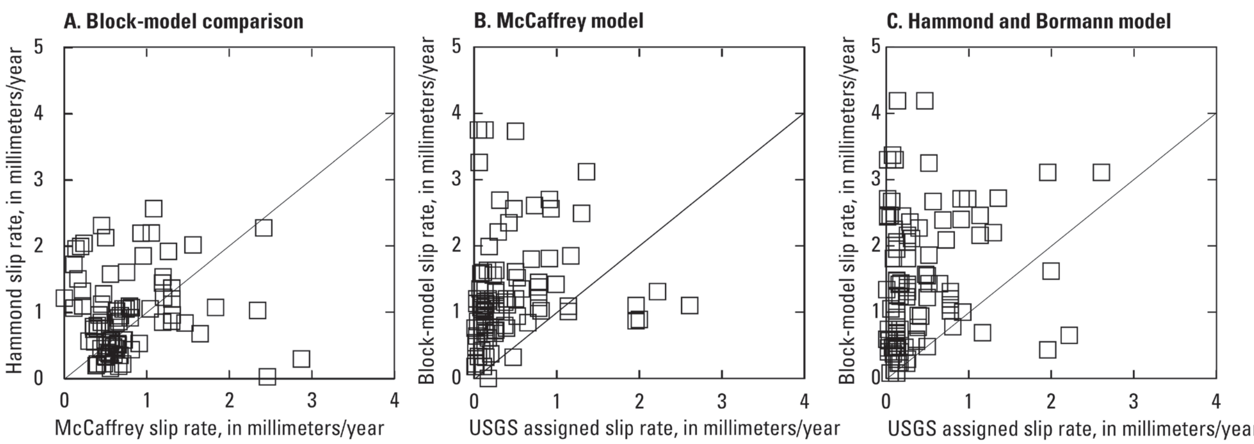

Figure A-5. Comparison of fault slip rates (total rate) for *A,* McCaffrey (appendix A) and Hammond and Bormann (appendix B) block models and slip rates for the modified 2008 fault source model compared to the *B,* McCaffrey (appendix A) block model, and the *C,* Hammond and Bormann (appendix B) block model.

Internal Block Strain Rates

Along with the rotational components of the blocks, uniform strain rates are estimated for them (fig. A-6). The horizontal strain-rate tensor for a spherical Earth is given by Savage and others (2001)—the east and north velocities are as follows:

$$V_\lambda (\lambda, \theta) = e_{\lambda\lambda} R_e \sin \theta_o (\lambda - \lambda_o) + e_{\lambda\theta} R_e (\theta - \theta_o)$$

$$V_\theta (\lambda, \theta) = e_{\lambda\theta} R_e \sin \theta_o (\lambda - \lambda_o) + e_{\theta\theta} R_e (\theta - \theta_o) \qquad (4)$$

where λ is longitude, θ is co-latitude, R_e is the radius of the Earth, e_{ij} is the strain-rate tensor, and (λ_o, θ_o) is the centroid of the block. When applied, the three independent components of the symmetric strain-rate tensor, $e_{\lambda\lambda}$, $e_{\theta\theta}$, and $e_{\lambda\theta}$, are formally estimated in the inversion (McCaffrey, 2005). These terms are intended to represent deformation due to unmodeled faults within the blocks. In the WUS outside California, the internal strain rates are generally low, less than 10 nanostrain/year (1 nanostrain/year = 10^{-9} year^{-1}). The fastest straining regions are the Yakima fold-thrust belt in Washington and parts of the Basin and Range (fig. A-6).

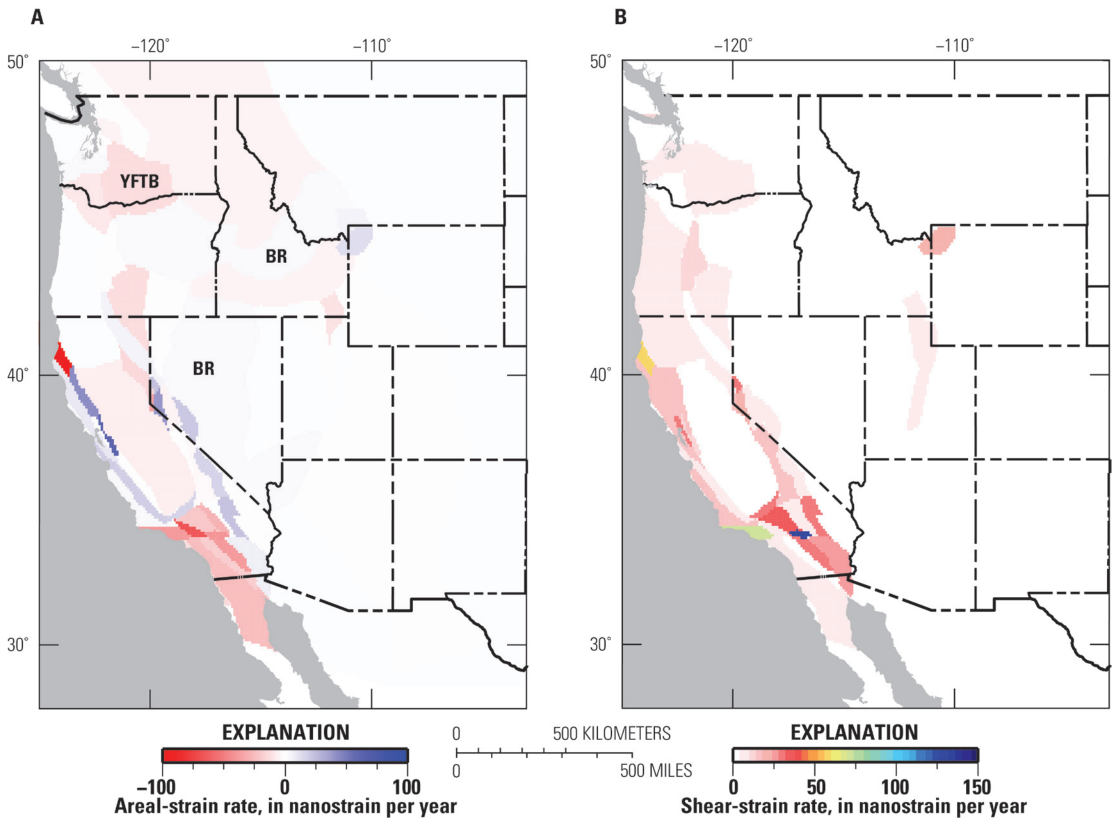

Figure A-6. Maps of *A,* areal strain rate and *B,* shear strain rate within blocks estimated from global positioning system data and the inversion program *tdefnode*. BR = Basin and Range; YFTB = Yakima fold-thrust belt. Negative strain rates are contraction and positive are extension.

Summary

A working group developed a block model for the WUS to incorporate GPS data into the assessment of slip rates to be adopted by NSHMP14. The model was run through two separate codes and predicted slip rates for a subset of the 2014 source faults. The block models showed considerable scatter in their agreement on slip rates, but both were consistently faster than the adopted geologic slip rates from expert analysis. The WUS outside California poses a particular difficulty for geodetic methods to contribute to hazards assessment due to the low density of GPS stations and low slip rates on faults. Continued densification of the geodetic networks and longer observation spans, to reduce errors, will enhance the utility of GPS for earthquake hazards assessment.

References Cited

Bird, Peter, 2007, Uncertainties in long-term geologic offset rates of faults—General principles illustrated with data from California and other Western States: Geosphere, v. 3, p. 577–595, doi: 10.1130/GES00127.1.

Burgette, R.J., Weldon, R.J., and Schmidt, D.A., 2009, Interseismic uplift rates for western Oregon and along-strike variation in locking on the Cascadia subduction zone: Journal of Geophysical Research, v. 114, B01408, doi:10.1029/2008JB005679.

DeMets, Charles, Gordon, R.G., and Argus, D.F., 2010, Geologically current plate motions: Geophysical Journal International, doi: 10.1111/j.1365-246X.2009.04491.x

Haller, K.M., and Wheeler, R.L., 2008a, Parameter for faults in the Intermountain West, *in* Peterson, M.D., Frankel, A.D., Harmsen, S.C., Mueller, C.S., Haller, K.M., Wheeler, R.L., Wesson, R.L., Zeng, Yuehua, Boyd, O.S., Perkins D.M., Luco, Nico, Field, E.H., Wills, C.J., and Rukstales, K.S., Documentation for the 2008 update of the national seismic hazard maps: U.S. Geological Survey Open-File Report 2008–1128, p. G-1–G-18.

Haller, K.M., and Wheeler, R.L., 2008b, Parameter for faults in the Pacific Northwest, *in* Peterson, M.D., Frankel, A.D., Harmsen, S.C., Mueller, C.S., Haller, K.M., Wheeler, R.L., Wesson, R.L., Zeng, Yuehua, Boyd, O.S., Perkins D.M., Luco, Nico, Field, E.H., Wills, C.J., and Rukstales, K.S., Documentation for the 2008 update of the national seismic hazard maps: U.S. Geological Survey Open-File Report 2008–1128, p. H-1–H-6.

Hammond, W.C., Blewitt, Geoffrey, and Kreemer, Corné, 2011, Block modeling of crustal deformation of the northern Walker Lane and Basin and Range from GPS velocities: Journal of Geophysical Research, v. 116, B04402, doi:10.1029/2010JB007817.

Kreemer, Corné, Blewitt, Geoffrey, and Hammond, W.C., 2010, Evidence for an active shear zone in southern Nevada linking the Wasatch fault to the eastern California shear zone: Geology, v. 38, p. 475–478, doi: 10.1130/G30477.1.

McCaffrey, Robert, 2002, Crustal block rotations and plate coupling, *in* Stein, Seth, and Freymueller, Jeffrey, eds., Plate boundary zones: AGU Geodynamics Series 30, p. 101–122.

McCaffrey, Robert, 2005, Block kinematics of the Pacific-North America plate boundary in the southwestern US from inversion of GPS, seismological, and geologic data: Journal of Geophysical Research, v. 110, B07401, doi:10.1029/2004JB003307.

McCaffrey, Robert, 2009, Time-dependent inversion of three-component continuous GPS for steady and transient sources in northern Cascadia: Geophysical Research Letters, v. 36, L07304, doi:10.1029/2008GL036784.

McCaffrey, Robert, Qamar, A.I., King, R.W., Wells, Ray, Khazaradze, Giorgi, Williams, C.A., Stevens, C.W., Vollick, J.J., and Zwick, P.C., 2007, Fault locking, block rotation and crustal deformation in the Pacific Northwest: Geophysical Journal International, v. 169, p. 1315–1340, doi:10.1111/j.1365-246X.2007.03371.x.

McCaffrey, Robert, King, R.W., Payne, S.J., and Lancaster, Matthew, 2013, Active tectonics of northwestern US inferred from GPS-derived surface velocities: Journal of Geophysical Research, v. 118, doi:10.1029/2012JB009473.

McCrory, P.A., Blair, J.L., Oppenheimer, D.H., and Walter, S.R., 2003, Depth to the Juan de Fuca slab beneath the Cascadia subduction margin—A 3-D model for sorting earthquakes: U.S. Geological Survey Digital Data Series 91, 1 CD-ROM.

Meade, B.J., and Hager, B.H., 2005, Block models of crustal motion in southern California constrained by GPS measurements: Journal of Geophysical Research, v. 110, doi:10.1029/2004JB003209.

Okada, Yoshimitsu, 1985, Surface deformation due to shear and tensile faults in a half-space: Bulletin of the Seismological Society of America, v. 75, p. 1135–1154.
Payne, S.J., McCaffrey, Robert, and King, R.W., 2008, Strain rates and contemporary deformation in the Snake River Plain and surrounding Basin and Range from GPS and seismicity: Geology, v. 36, p. 647–650.
Payne, S.J., McCaffrey, Robert, King, R.W., and Kattenhorn, S.A., 2012, A new interpretation of deformation rates in the Snake River Plain and adjacent Basin and Range regions based on GPS measurements: Geophysical Journal International, v. 189, p. 101–122, doi: 10.1111/j.1365-246X.2012.05370.x.
Savage, J.C., 1983, A dislocation model of strain accumulation and release at a subduction zone: Journal of Geophysical Research, v. 88, p. 4984–4996.
Savage, J.C., Gan, Weijun, and Svarc, J.L., 2001, Strain accumulation and rotation in the eastern California shear zone: Journal of Geophysical Research, v. 106, p. 21,995–22,007.
Shen, Z-K., King, R.W., Agnew, D.C., Wang, M., Herring, T.A., Dong, D., and Fang, P., 2011, A unified analysis of crustal motion in southern California, 1970–2004—The SCEC crustal motion map: Journal of Geophysical Research, v. 116, doi: 10.2019/2011JB008549.
Wang, K., Wells, R., Mazzotti, S., Hyndman, R.D., and Sagiya, T., 2003, A revised dislocation model of interseismic deformation of the Cascadia subduction zone: Journal of Geophysical Research, v. 108, 2026, doi:10.1029/2001JB001227.

Appendix B—A Block Model of Western United States Tectonic Deformation for the 2014 National Seismic Hazard Maps from GPS and Geologic Data

By William C. Hammond[1] and Jayne Bormann[2]

[1]Nevada Geodetic Laboratory, Nevada Bureau of Mines and Geology and Nevada Seismological Laboratory, Reno, Nev.
[2]University of Nevada, Reno, Nev.

Abstract

We have constructed a kinematic model of Western United States (WUS) tectonic deformation using the same block geometry and GPS velocity data used in appendix A. The methodology is conceptually similar to that used in the McCaffrey model (appendix A), using GPS velocities and geologic slip rates as constraints on a block model of crustal deformation patterns. Differences in methods include using a different software and model regularization to solve for the rotations of individual blocks and fault slip rates and employing a viscoelastic seismic-cycle model to account for postseismic relaxation of earthquakes in Nevada. Although the resulting model is similar in its deformation patterns to the McCaffrey block model, individual slip-rate estimates differ in many cases. In our modeling we allow for constant tensor strain rates inside large blocks, but our regularization results in a model with more deformation assigned to block-bounding slip rates and less to the interior of large blocks compared to the other models. Throughout the interior of the WUS, the slip rates in our model are on average greater than the geologic slip rates.

Introduction

We have developed a kinematic model of crustal deformation of the Western United States (WUS) in order to constrain the geographic distribution of hazard from earthquakes. The purpose of this modeling is to apply the rich and growing dataset of global positioning system (GPS) velocities from several research groups and facilities to obtain a model of deformation that is kinematically consistent and treats all observations uniformly. The model is designed to estimate slip rates on active faults that bound individual blocks of the crust and distribute the remaining deformation within the block interiors. In the model, the blocks move horizontally via rotations described by Euler poles (McKenzie and Parker, 1967) at rates with a sense of rotation that are constrained by a compilation of GPS measurements of horizontal velocity with respect to North America.

Our model is a companion to the model presented by McCaffrey (appendix A). We use the same block geometry, including assumed values for fault-locking depth and fault dips. We also use the same velocity data including correction for interseismic locking on the Cascadia subduction zone. The problem is solved with methodology and software developed at the Nevada Geodetic Laboratory that has been used extensively to estimate crustal motions from GPS observations (Hammond and Thatcher, 2007; Hammond and others, 2011). Though many of the model features are similar to the McCaffrey block model, differences in methodology lead to slightly different results. The degree of similarity between our model and the McCaffrey model shows the degree of repeatability of the results and evaluates the stability of the analysis with respect to modeling technique.

We use the geologic estimates of fault slip rates provided by the U.S. Geological Survey (Haller and Wheeler, 2008a,b) as additional data to constrain our model. However, the weighting placed on the geologic slip rate observations is less than that placed on the GPS data, so that deformation is driven primarily by geodetic observations and secondarily by geologic observations. The weight placed on geologic observations is less than in some of the other deformation models (for example, Bird, appendix C, and Zeng and Shen, appendix D). Compared to those models, our model is more likely to reflect contemporary deformation from decadal time-scale measurements and may not be the same as those estimated from longer periods of geologic time.

We allowed strain to occur inside most of the larger blocks, allowing uniform three-component horizontal tensor strain rate representing distributed permanent deformation. However these parameters were damped toward zero, so their contribution to the overall model velocity field was kept to near the minimum necessary to explain the data. Thus, our model explains the data with a deformation field that places more emphasis on the slip on the discrete fault systems at block boundaries; that is, it is “blockier” than the other models. The other deformation models used parameterizations that allowed a greater proportion of the overall deformation budget to occur inside blocks and hence have a greater amount of continuum deformation in addition to slip on block-bounding faults.

Data

We used the same combination of GPS velocity fields as McCaffrey (appendix A) and the same correction for the effects of the Cascadia subduction zone interseismic locking. This correction has a large effect (>10 mm/yr) on the velocities near the Oregon and Washington coasts, replacing eastward interseismic motion with more oceanward long-term motion (McCaffrey and others, 2013). The magnitude of the correction decreases rapidly eastward where the rates are less affected by interseismic locking on the subduction zone plate interface.

We exclude velocity data that do not represent the long-term deformation-field-associated loading of earthquake faults. In particular, we omitted data near active volcanic systems (Long Valley, Lassen Peak, and Mount Shasta in California, Mount Saint Helens in Washington). We also removed velocity outliers that were more than 4 mm/yr different than the interpolated expectation based on other velocities within a 25-km radius. Finally, we averaged duplicate velocities from individual GPS stations present in the combined velocity file that were essentially multiple velocity estimates from the same data. The outlier detection removed less than 2 percent of the velocities.

The upper mantle and lower crust in the WUS have viscoelastic material properties and experience transient deformation following large historic earthquakes (see for example, Pollitz and others, 2000). For this analysis we applied a correction to account for viscoelastic relaxation following large historic earthquakes in Nevada and eastern California. Because of lower tectonic strain rates in the Great Basin, the transient early-cycle deformation from these earthquakes stands out more readily from the background than elsewhere in the Pacific-North America plate boundary (Hammond and Thatcher, 2004; Hammond and others, 2012) leading to the potential for proportionally larger bias of slip rates in Nevada. This correction was developed from models of the 1872 Owens Valley, 1915 Pleasant Valley, 1932 Cedar Mountain, 1954 Rainbow Mountain/Stillwater sequence, 1954 Fairview Peak, and 1954 Dixie Valley earthquakes (Hammond and others, 2009). Applying this model reduces the inferred normal component of the slip rate for the large blocks in Nevada east and west of the Dixie Valley fault (blocks WBnR and CBnR, fig. A-1). Hammond and others (2011, their fig. 5) depict this correction graphically. To apply the correction, we subtract the modeled transient velocities from the GPS velocities to estimate a late cycle rate that is similar to the cycle-averaged rate in the slowly deforming Basin and Range.

Method

Block modeling is a method by which geodetic measurements made over a few years of interseismic time can be used to infer the motion of blocks of crust over times applicable to seismic hazard analysis, that is, over the next few seismic cycles. This time period is essentially instantaneous in the context of plate tectonics. The analytical details vary somewhat between the different approaches that have been discussed in previous studies (some examples include Matsu'ura and others, 1986; Bennett and others, 1996; Prawirodirdjo and others, 1997; McClusky and others, 2001; Murray and Segall, 2001; McCaffrey, 2002; Meade and Hager, 2005; Reilinger and others, 2006; McCaffrey and others, 2007). These are conceptually similar in that they account for block motion and fault locking. Our model accounts for the difference between the long- and short-term velocity field by applying back-slip (Savage, 1983), estimating the elastic strain owing to block-boundary fault segments using the formulation of Okada (1985).

The model geometry is shown in detail in appendix A. It includes known major faults in the WUS from Colorado westward to the Pacific plate and extends south and north into Mexico and Canada. We used the prescribed values for fault dips and locking depths.

The model regularization is similar to that used in the northern Walker Lane model of Hammond and others (2011). In that model, the damping of slip rates and vertical-axis spin rates causes poorly constrained blocks to move in a direction similar to neighboring blocks. Compared to that model, however, the WUS model has a greater number of GPS observations, larger blocks, a greater variety of slip rates, and better constraints on the motions of large blocks at the boundaries of the model. Thus for this WUS model, we relax the block vertical-axis spin-rate damping (10^{-7}/yr) and the *a priori* uncertainty on slip rates (30 mm/yr), but otherwise keep all material properties the same. This regularized approach makes the model tolerant to small gaps in data coverage because blocks will follow the averaged behavior of neighboring blocks in the absence of data. In the WUS model, all blocks had at least one GPS station, and only two blocks had fewer than five GPS stations.

In addition to block rotation and fault locking, we allowed a subset of the blocks to experience constant horizontal-tensor strain rate if demanded by the data. We allowed strain in all large blocks (blocks with areas greater than 20,000 km^2) except for the JdFa, Paci, Josh, WCCR, and EWkL blocks (fig A-1). The Paci and JdFa blocks had rotations poles fixed to values in the literature (Kreemer and others, 2000; McCaffrey and others, 2007) because they had insufficient GPS velocities on those blocks to constrain block motion.

We applied geologic data provided by the USGS (updated from Haller and Wheeler, 2008a,b) as additional constraints on the blocks motions. For each fault segment in the model, we selected the nearest geologic slip rate and used the slip rate as a constraint if it was within 5 km of the model segment. Slip rates in the model were set to the geologic slip rates, distributed to the appropriate components (dip-slip or strike-slip) using the rake information supplied in the USGS file. We regularized the importance of the geologic slip-rate constraint by setting the *a priori* uncertainty in the model slip rate. After testing several choices, we selected a value that placed a weaker (but greater than zero) emphasis on geologic slip rates. This had the effect of constraining the model mostly by GPS data but stabilizing the model where GPS data were weak.

Additional tests of the modeling were performed to determine if the solution was stable with respect to specific factors. In one test we used an independent GPS velocity field, generated by the Nevada Geodetic Laboratory, to see if homogenous processing using only continuous and semicontinuous stations would improve the model. We found that a model generated using this velocity field had fewer outliers, but it fit the data only slightly better than the velocities used for this model. This suggested that the limitations to fitting the GPS data are likely attributable to the relative simplicity of the block geometries where a small number of large blocks and constant strain rates are used to explain a large and complex plate boundary deformation zone.

Results and Discussion

The results of our modeling are shown in figure B-1. Most blocks spin around vertical axes at rates between 2° clockwise and 1° counterclockwise per million years, with lower rates in the Intermountain West and Basin and Range and higher rates with a variable sign inside the San Andreas and Cascadia plate boundary zones. The root mean square (RMS) misfits of the model to the GPS data are near 1.3 and 1.4 mm/yr in the east and north components, respectively (fig. B-2). The misfits tend to be higher in regions where (1) slip rates are higher and deformation patterns are more complex (for example, near the creeping sections of the San Andreas Fault in California) and (2) recent large earthquakes are distorting the GPS velocity field with unmodeled transient deformations (for example, around the 1999 Hector Mine and 1992 Landers earthquakes). The normalized chi-squared misfit values for the entire model, including both north and east components of GPS velocity (but excluding velocities that were omitted as outliers as discussed above) is 8.46. However, considering only data outside of California results in a smaller normalized chi-square of 3.48 (table B-1). The difference in misfits between our and the other models is likely attributable to the difference in number of parameters, modeling style, and method of outlier detection and removal.

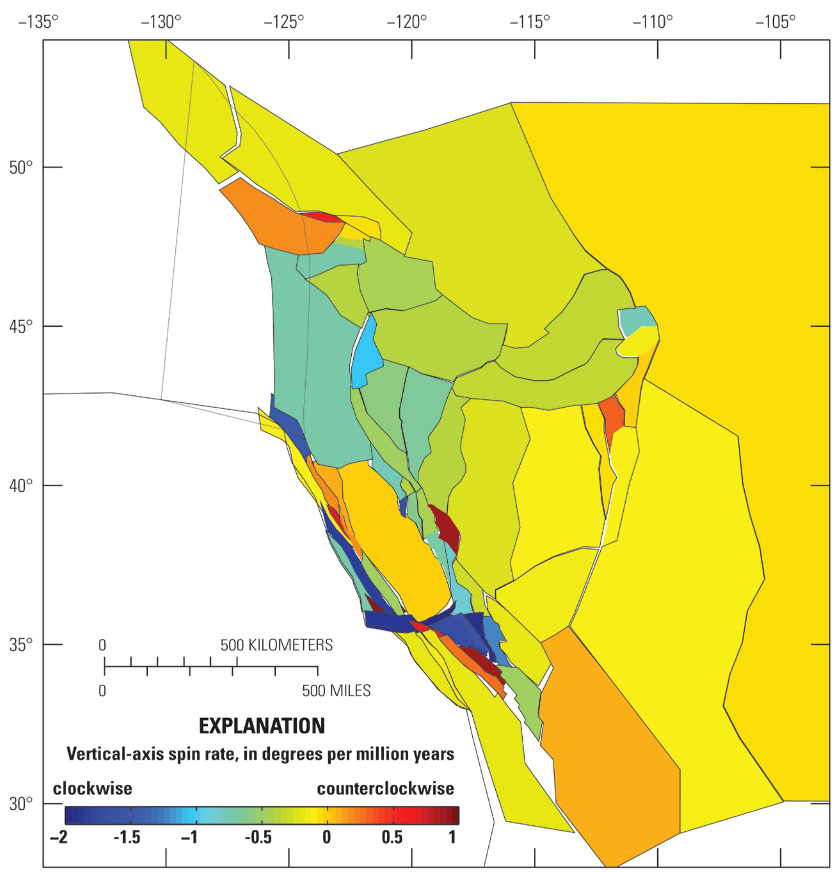

Figure B-1. Rotation of blocks in the model. Color represents vertical-axis spin rate of blocks in the model. The displacement of blocks represents the long-term horizontal block motion greatly exaggerated. The Juan de

Fuca and Pacific blocks (see fig. A-1 JdFa and Paci, respectively) have been made transparent to better show blocks near the coast. Magenta lines represent the original position of the blocks.

Table B-1. Misfit of model to data.

[RMS, root mean square]

Misfit to GPS data	Entire Western U.S. model	Outside California
Number of GPS observations (sites times 2)	5,790	3,134
RMS of residual velocities (mm/yr)	1.32	0.90
Normalized chi-square (unitless, 1.0 ideal)	8.46	3.48
Number of model parameters	267	
Reduced chi-square (unitless, 1.0 ideal)	8.87	3.81

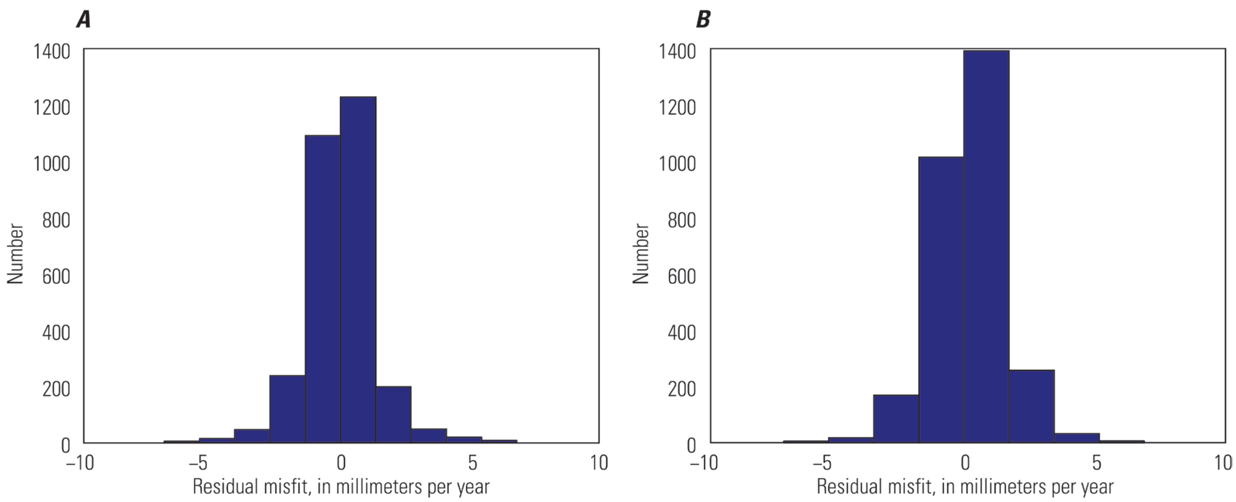

Figure B-2. Plots of residual misfit between global positioning system velocities and predictions from block model *A,* east residuals and *B,* north residuals.

As discussed in appendix A, our model is more "blocky" in the sense that the deformation partitioned to the interior of blocks is less than in the McCaffrey block model (appendix A), and less than in the continuum models of Zeng and Shen (appendix D) and Bird (appendix C). In this respect, our model is an end member that places more slip on faults and concentrates deformation at the known active faults. Future versions of this modeling could be improved by increasing the number of blocks and (or) by allowing more deformation to be partitioned into block interiors. However, when allowing more deformation inside blocks, the hazard will need to be accounted for as distributed source zones that abide by the budget of seismogenic moment across the WUS.

In both block models, the geodetic slip rates are on average greater than the geologic rates (fig. A-5). That comparison is made for faults outside California that slip at rates much slower than individual slip rates in the San Andreas Fault system (fig. B-3). Possible reasons for these disagreements include, but may not be limited to, (1) geometric simplicity of the block model so its ability to fit GPS data is limited, (2) strike-slip deformation on slowly moving faults is systematically underrepresented in the database of geologic slip rates because it is more difficult to observe in the geologic record, (3) geologic slip rates are estimated without the constraint of regional kinematic consistency so their uncertainties are underestimated, (4) the time scales to which geodetic (10^1 years) and geologic data (10^2 to 10^5 years) are sensitive are different, and slip rates have changed over time (see for example, Friedrich and others, 2003; Bennett, 2007). Thus, the disagreements between geologic and geodetic slip rates may represent a combination of real variation and aleatory and epistemic uncertainties in the geographic distribution of tectonic deformation.

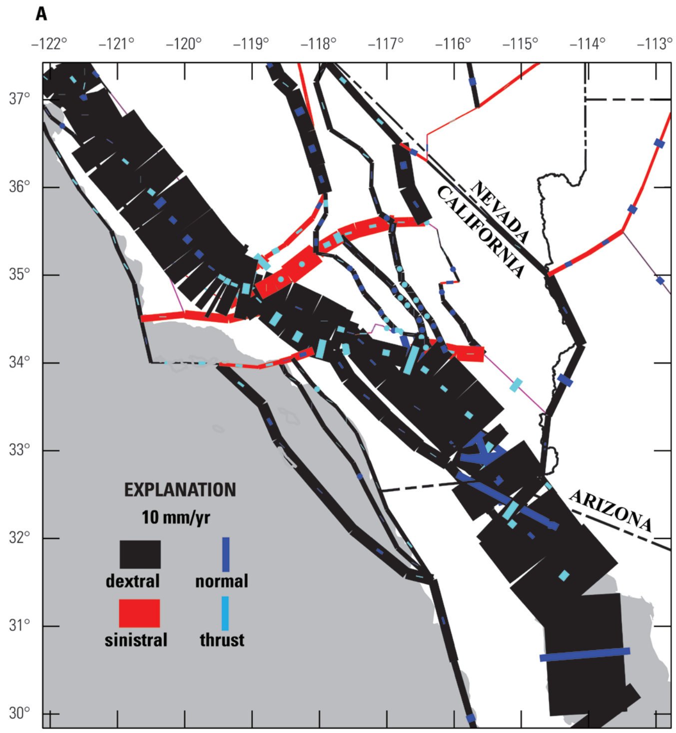

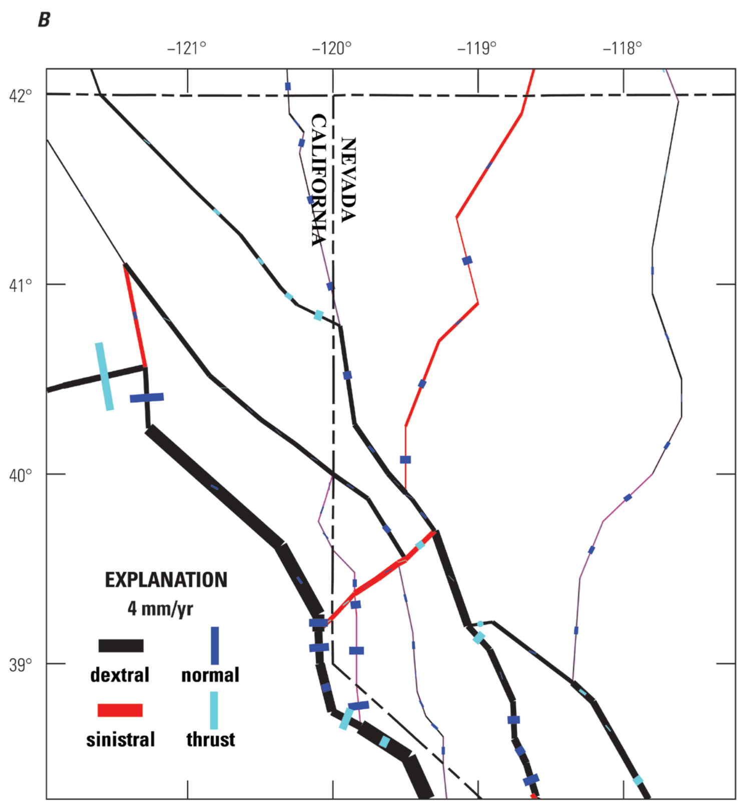

Figure B-3. Close-up of the model in the *A,* southern California and *B,* northern Walker Lane regions. In *A,* slip rates are shown on faults between western Arizona, southern Nevada, and the Pacific plate. In *B,* the slip rates in northeast California and northwest Nevada are much lower, and a different scale is used. Thickness of black and red lines shows dextral and sinistral slip rates, respectively. Length of blue and cyan lines indicates horizontal component of normal and thrust rates, respectively.

References Cited

Bennett, R.A., Rodi, William, and Reilinger, R.E., 1996, Global positioning system constraints on fault slip rates in southern California and northern Baja, Mexico: Journal of Geophysical Research, v. 101, no. B10, p. 21,943–21,960.

Bennett, Richard, 2007, Instantaneous slip rates from geology and geodesy: Geophysical Journal International, v. 169, p. 19–28, doi: 10.1111/j.1365-246X.2007.03331.x.

Friedrich, A.M., Wernicke, B.P., Niemi, N.A., Bennett, R.A., and Davis, J.L., 2003, Comparison of geodetic and geologic data from the Wasatch region, Utah, and implications for the spectral character of Earth deformation at periods of 10 to 10 million years: Journal of Geophysical Research, v. 108, no. B4, 2199, doi:10.1029/2001JB000682.

Haller, K.M., and Wheeler, R.L., 2008a, Parameter for faults in the Intermountain West, *in* Peterson, M.D., Frankel, A.D., Harmsen, S.C., Mueller, C.S., Haller, K.M., Wheeler, R.L., Wesson, R.L., Zeng, Yuehua, Boyd, O.S., Perkins D.M., Luco, Nico, Field, E.H., Wills, C.J., and Rukstales, K.S., Documentation for the 2008 update of the national seismic hazard maps: U.S. Geological Survey Open-File Report 2008–1128, p. G-1–G-18.

Haller, K.M., and Wheeler, R.L., 2008b, Parameter for faults in the Pacific Northwest, *in* Peterson, M.D., Frankel, A.D., Harmsen, S.C., Mueller, C.S., Haller, K.M., Wheeler, R.L., Wesson, R.L., Zeng, Yuehua, Boyd, O.S., Perkins D.M., Luco, Nico, Field, E.H., Wills, C.J., and Rukstales, K.S., Documentation for the 2008 update of the national seismic hazard maps: U.S. Geological Survey Open-File Report 2008–1128, p. H-1–H-6.

Hammond, W.C., and Thatcher, Wayne, 2004, Contemporary tectonic deformation of the Basin and Range Province, Western United States—10 years of observation with the global positioning system: Journal of Geophysical Research, v. 109, B08403, doi:10.1029/2003JB002746.

Hammond, W.C., and Thatcher, Wayne, 2007, Crustal deformation across the Sierra Nevada, northern Walker Lane, Basin and Range transition, Western United States measured with GPS, 2000–2004: Journal of Geophysical Research, v. 112, B05411, doi:10.1029/2006JB004625.

Hammond, W.C., Kreemer, Corné, and Blewitt, Geoffrey, 2009, Geodetic constraints on contemporary deformation in the northern Walker Lane—3, Central Nevada seismic belt postseismic relaxation, *in* Oldow, J.S., and Cashman, P.H., eds., Late Cenozoic structure and evolution of the Great Basin-Sierra Nevada transition: Geological Society of America Special Paper 447, p. 33–54.

Hammond, W.C., Blewitt, Geoffrey, and Kreemer, Corné, 2011, Block modeling of crustal deformation of the northern Walker Lane and Basin and Range from GPS velocities: Journal of Geophysical Research, v. 116, B04402, doi:10.1029/2010JB007817.

Hammond, W.C., Blewitt, Geoffrey, Li, Zhenhong, Plag, H.-P., Kreemer, Corné, 2012, Contemporary uplift of the Sierra Nevada, Western United States, from GPS and InSAR measurements: Geology, v. 40, p. 667–670, doi:10.1130/G32968.1.

Kreemer, Corné, Haines, John, Holt, W.E., Blewitt, Geoffrey, and Lavallée, David, 2000, On the determination of the global strain rate model: Earth Planets Space, v. 52, p. 765–770.

Matsu'ura, Mitsuhiro, Jackson, D.D., and Cheng, Abe, 1986, Dislocation model for aseismic crustal deformation at Hollister, California: Journal of Geophysical Research, v. 91, no. B12, p. 12,661–12,674.

McCaffrey, Robert, 2002, Crustal block rotations and plate coupling, *in* Stein, S.A., and Freymueller, J.T., eds., Plate boundary zones: AGU Geodynamics Series, v. 30, p. 101–122.

McCaffrey, Robert, Qamar, A.I., King, R.W., Wells, Ray, Khazaradze, Giorgi, Williams, C.A., Stevens, C.W., Vollick, J.J., and Zwick, P.C., 2007, Fault locking, block rotation and crustal deformation in the

Pacific Northwest: Geophysical Journal International, v. 169, p. 1315–1340, doi:10.1111/j.1365-246X.2007.03371.x.
McCaffrey, Robert, King, R.W., Payne, S.J., and Lancaster, Matthew, 2013, Active tectonics of northwestern US inferred from GPS-derived surface velocities: Journal of Geophysical Research, v. 118, doi:10.1029/2012JB009473.
McClusky, S.C., Bjornstad, S.C., Hager, B.H., King, R.W., Meade, B.J., Miller, M.M., Monastero, F.C., and Souter, B.J., 2001, Present day kinematics of the eastern California shear zone from a geodetically constrained block model: Geophysical Research Letters, v. 28, p. 3369–3372.
McKenzie, D.P., and Parker, R.L., 1967, The north Pacific—An example of tectonics on a sphere: Nature, v. 216, p. 1276–1280.
Meade, B.J., and Hager, B.H., 2005, Block models of crustal motion in southern California constrained by GPS measurements: Journal of Geophysical Research, v. 110, B03403, doi:10.1029/2004JB003209.
Murray, M.H., and Segall, Paul, 2001, Modeling broad scale deformation in northern California and Nevada from plate motions and elastic strain accumulation: Geophysical Research Letters, v. 28, p. 4315–4318.
Okada, Yoshimitsu, 1985, Surface deformation due to shear and tensile faults in a half-space: Bulletin of the Seismological Society of America, v. 75, p. 1135–1154.
Pollitz, F.F., Peltzer, Gilles, and Bürgmann, Roland, 2000, Mobility of continental mantle—Evidence from postseismic geodetic observation following the 1992 Landers earthquake: Journal of Geophysical Research, v. 105, p. 8035–8054.
Prawirodirdjo, L., Bocl, Y., McCaffrey, R., Genrich, J., Calais, E., Stevens, C., Puntodewo, S.S.O., Subarya, C., Rais, J., Zwick, P., and Fauzi, R.M., 1997, Geodetic observations of interseismic strain segmentation at the Sumatra subduction zone: Geophysical Research Letters, v. 24, p. 2601–2604.
Reilinger, Robert, McClusky, Simon, Vernant, Philippe, Lawrence, Shawn, Ergintav, Semih, Cakmak, Rahsan, Ozener, Haluk, Kadirov, Fakhraddin, Guliev, Ibrahim, Stepanyan, Ruben , Nadariya, Merab, Hahubia, Galaktion, Mahmoud, Salah, Sakr, K., ArRajehi, Abdullah, Paradissis, Demitris, Al-Aydrus, A., Prilepin, Mikhail, Guseva, Tamara, Evren, Emre, Dmitrotsa, Andriy, Filikov, S.V., Gomez, Francisco, Al-Ghazzi, Riad, Karam, Gebran, 2006, GPS constraints on continental deformation in the Africa-Arabia-Eurasia continental collision zone and implications for the dynamics of plate interactions: Journal of Geophysical Research, v. 111, B05411, doi:10.1029/2005JB004051.
Savage, J.C., 1983, A dislocation model of strain accumulation and release at a subduction zone: Journal of Geophysical Research, v. 88, p. 4984–4996.